**PAPER** • **OPEN ACCESS**

# Acetylcholine-loaded nanoparticles protect against doxorubicin-induced toxicity in *in vitro* cardiac spheroids

To cite this article: Clara Liu Chung Ming *et al* 2025 *Biofabrication* **17** 025023

Biofabrication

PAPER

# Acetylcholine-loaded nanoparticles protect against doxorubicin-induced toxicity in *in vitro* cardiac spheroids

**Clara Liu Chung Ming**[1,2], **Runali Patil**[3,4,5], **Ahmed Refaat**[5,6,7], **Sean Lal**[8], **Xiaowei Wang**[4,5,6] and **Carmine Gentile**[1,2,*]

[1] School of Biomedical Engineering, Faculty of Engineering and Information Technology, University of Technology Sydney, Sydney, NSW, Australia
[2] Cardiovascular Regeneration Group, Heart Research Institute, Newtown, NSW 2042, Australia
[3] IIT-Bombay Monash Research Academy, IIT Bombay, Powai, Mumbai, Maharashtra 400076, India
[4] Department of Medicine, Monash University, Melbourne, VIC 3800, Australia
[5] Molecular Imaging and Theranostics Laboratory, Baker Heart and Diabetes Institute, Melbourne, VIC 3004, Australia
[6] Department of Cardiometabolic Health, University of Melbourne, Melbourne, VIC 3010, Australia
[7] Department of Drug Delivery Disposition and Dynamics, Monash Institute of Pharmaceutical Sciences, Monash University, Melbourne, VIC 3052, Australia
[8] School of Medical Sciences, Faculty of Medicine and Health, University of Sydney, Camperdown, NSW 2050, Australia
[*] Author to whom any correspondence should be addressed.

**E-mail:** carmine.gentile@uts.edu.au

**Keywords:** doxorubicin, 3D *in vitro* modeling, cardiac spheroids, acetylcholine, nanoparticles

Supplementary material for this article is available online

OPEN ACCESS

RECEIVED
9 October 2024

REVISED
28 January 2025

ACCEPTED FOR PUBLICATION
18 February 2025

PUBLISHED
7 March 2025



## Abstract

Doxorubicin (DOX) is widely used in chemotherapy, yet it significantly contributes to heart failure-associated death. Acetylcholine (ACh) is cardioprotective by enhancing heart rate variability and reducing mitochondrial dysfunction and inflammation. Nonetheless, the protective role of ACh in countering DOX-induced cardiotoxicity (DIC) remains underexplored as current approaches to increasing ACh levels are invasive and unsafe for patients. In this study, we explore the protective effects of ACh against DIC through three distinct ACh administration strategies: (i) freely-suspended 100 $\mu$M ACh; (ii) ACh-producing cholinergic neurons (CNs); or (iii) ACh-loaded nanoparticles (ACh-NPs). These are tested in *in vitro* cardiac spheroids (CSs), which have previously been shown to approximate the complex DIC. We assess ACh's protective effects by measuring the toxicity ratio (cell death/viability), contractile activity, gene expression changes via qPCR and nitric oxide (NO) signaling. Our findings show that ACh effectively attenuates DOX-induced cell death and contractile dysfunction. ACh also counteracts the DOX-induced downregulation of genes controlling myocardial fibrosis, endothelial and cardiomyocyte dysfunction, and autonomic dysregulation. ACh cardioprotection against DOX is dependent on NO signaling in endothelial cells but not in cardiac myocytes or fibroblasts. Altogether, this study shows for the first time that elevating ACh levels showed a promising therapeutic approach for preventing DIC.

## 1. Introduction

Doxorubicin (DOX) is an antineoplastic agent extensively employed in treating various types of cancer, such as leukemia, lymphoma, and others [1, 2]. Despite its clinical utility in oncology, DOX is notoriously associated with chronic cardiotoxicity, and it is estimated that up to 65% of oncology patients may experience DOX-induced cardiotoxicity (DIC). This leads to adverse cardiac outcomes, including reduced left ventricular ejection fraction, ventricular wall thickening, arrhythmias, and congestive heart failure (HF) [2, 3]. The mechanisms involved in DIC include inhibition of autophagy, DNA/RNA damage, nitric oxide (NO) release, endothelial dysfunction, increase of inflammatory mediators, and cell death [4]. While NO produced at a standard dose in the heart maintains cardiac function and exerts anti-apoptotic effects, excess NO in endothelial cells can be detrimental, leading to cardiac dysfunction

associated with increased cardiomyocyte death and endothelial dysfunction [5]. Previous studies utilizing cardiac spheroids (CSs) models have elucidated that DIC is mechanistically linked to NO synthesis, through the activation of endothelial nitric oxide synthase (eNOS) via its phosphorylation, facilitating superoxide generation [6]. DOX-mediated redox activation of eNOS has been implicated in cardiac apoptosis and eNOS-dependent reactive oxygen species (ROS) generation, significantly contributing to myocardial dysfunction [7]. Additionally, we previously showed that DOX increased necrotic death of cardiac cells and reduced contractility function in CS via NOS signaling in cardiac endothelial cells and fibroblasts [8].

Previous studies have demonstrated the critical role played by the neurotransmitter acetylcholine (ACh) in regulating cardiovascular health for maintaining cardiac homeostasis [9–11]. Unbalance in ACh levels is characterized by sympathetic overactivation and parasympathetic deterioration, exacerbating cardiac mortality and impeding myocardial regeneration [12–14]. Kalay *et al* [15] demonstrated that carvedilol, a nonselective $\beta$-adrenoceptor antagonist, attenuated DOX-induced side effects and significantly improved the left ventricular function in patients. Additionally, Prathumsap *et al* [3] reported that activation of ACh receptors protected against DOX-induced myocardial inflammation and cardiomyocyte cell death and reduced ROS levels by preventing mitochondrial dysfunction. ACh has been shown to protect against myocardial infarction [16, 17], ischemic-reperfusion injury [18–21], diabetes [22] and heart failure [23, 24]. These cardioprotective effects are associated with the restoration of autonomic balance, reduction of heart rate variability, mitigation of mitochondrial dysfunction, and attenuation of inflammatory responses [14, 18, 25, 26]. Notably, recent studies have demonstrated ACh's efficacy in ameliorating DIC in rat models through the inhibition of NO synthase activity, diminution of DOX-induced apoptosis, and alleviation of mitochondrial dysfunction [27–29]. However, the long-term impact of DIC and the inadequacies of current *in vitro* and *in vivo* models of the human heart fail to capture the intricate pathophysiological landscape and fully underscore the necessity for advanced modeling techniques [30, 31].

This study employs CSs, 3D *in vitro* models of the human heart, which are composed of human-induced pluripotent stem cell-derived cardiomyocytes (iCMs), human coronary artery endothelial cells (HCAEC), and human cardiac fibroblasts (HCFs) [32]. Following our previous research showing the feasibility of testing DOX-induced toxicity in CSs, we, therefore, use them in this study to evaluate the protective effects of ACh against DIC. We hypothesize that ACh has protective effects against DOX-induced toxicity in CSs. ACh cardioprotection was tested using approaches: (*i*) either by adding freely-suspended ACh against DOX-treated CSs; (*ii*) or by adding ACh-producing iPSC-derived cholinergic neurons (CNs) to CSs (CN-CSs). To prevent ACh hydrolyses and its multitarget effects in the human body [33, 34], we developed novel ACh-loaded nanoparticles (ACh-NPs) made of poly-butylcyanoacrylate (PBCA) to deliver ACh in small doses and to target the injured area. PBCA-NPs have been thoroughly developed as a drug delivery system for cancer chemotherapy [35–37] and to pass through the brain-blood barrier [38, 39]. Wang *et al* [40] demonstrated that PBCA-NPs are safe, non-toxic, stable and can release the encapsulated drug in primary rat aortic endothelial cells to treat atherosclerosis. Given their unique properties, our third (*iii*) approach to delivering ACh was based on the addition of ACh-NPs to DOX-treated CS.

Our analytical approach to assess ACh cardioprotection included toxicity ratio measurements (dead/live cells), colocalization of a cell death marker in the three cell types, contractile activity, and gene expression analysis via qPCR. Furthermore, we aimed to juxtapose our DOX-treated CSs model with human heart tissue specimens, including healthy cardiac tissue, DOX cardiomyopathy, ischemic heart disease (IHD), and dilated cardiomyopathy (DCM), focusing on NOS signaling. This comprehensive study aims to elucidate the cardioprotective potential of ACh and to develop a novel and efficient therapeutic approach using ACh-NPs at the early stage of DIC.

## 2. Material and methods

The Human Ethics Committee of University of Technology Sydney and Sydney Human Heart Biobank, University of Sydney (HREC 2021/122), approved the use of human left ventricle myocardial tissue samples (UTS HREC REF NO. ETH21-5968, approved till 27/05/26). Human heart samples were from donor hearts that were not used for heart transplantation because of primarily logistical reasons. Anatomical pathology confirmed these tissues were normal. Heart failure samples were from patients with end-stage heart failure undergoing heart transplantation. Donor and heart failure samples were flash-frozen within 15 min of procurement.

### 2.1. Drugs and reagents

Cell culture: L-glutamine solution, penicillin-streptomycin and fibronectin bovine plasma were purchased from Sigma-Aldrich (catalogue number: G8540, P4458 and 10838039001, respectively). Cardiomyocytes iCell plating medium and iCell maintenance culture medium were purchased from Fujifilm Cellular Dynamics (catalog number: R1017). Laminin (Natural Mouse) was purchased from Thermo Fisher Scientific (catalog number:

23017015), and maintenance medium iN1(AP) was purchased from Elixirgen Scientific (catalog number: CH-MM).

Drugs: Acetylcholine chloride was used at 100 µM (catalog number: A266), Doxorubicin hydrochloride was used at a concentration of 10 µM (catalog number: D1515), and Atropine was used at 50 µM (catalog number: PHR3846) were purchased from Sigma-Aldrich.

Antibodies: Primary antibody purified mouse anti-human CD31 (BD Bioscience, catalog number: 550389) were used to immunolabelled HCAEC. Secondary antibody Alexa fluor® 647 affinipure™ goat anti-mouse IgG (H+L) (catalog number: 115-605-003), Alexa fluor® 790 affinipure™ Goat Anti-Mouse IgG (H+L) (catalog number: 115-655-146) and Alexa fluor® 647 affinipure™ Goat Anti-Rabbit IgG (H+L) (catalog number: 111-605-003) were purchased from Jackson ImmunoResearch. Alexa fluor® 488 mouse monoclonal (vimentin—cytoskeleton marker) was purchased from Abcam (catalog number: AB195877), and Troponin T-C (CT3) Alexa fluor® 546 was purchased from Santa Cruz (catalog number: sc-20025). Anti-choline acetyltransferase (ChAT) rabbit anti-human primary antibody from Sigma-Aldrich (catalog number: SAB5701171).

### 2.2. Generation of human cardiac spheroids (CSs) and CSs with cholinergic neuronal cells (CNs)

Human induced pluripotent stem cell-derived cardiomyocytes (iCMs) were obtained from Cellular Dynamics (catalog number: R1017). HCFs and human coronary artery endothelial cells (HCAEC) were purchased from Cell Applications, Inc. (catalog numbers: 306-05A and 300-05A, respectively). Cells were plated and cultured according to the supplier's instructions. Briefly, HCFs were cultured in cardiac fibroblast growth medium, and HCAECs were cultured in human MesoEndo Cell Growth Medium (Cell Applications, Inc, catalog number 316-500 and 212-500, respectively). L-glutamine–penicillin–streptomycin solution (1%) was added to both media for nutrient enrichment. According to the manufacturer's guidelines, iCMs were cultured in iCell plating medium and iCell maintenance culture medium in fibronectin pre-coated culture flasks (Cellular Dynamics, catalog number: R1017).

Human CSs were generated using the methodologies previously outlined [41, 42]. In summary, the monolayer cell cultures were passaged with trypsin-EDTA (Sigma-Aldrich; catalog number: T4049) and TrypLE™ Express Enzyme (Thermofisher Scientific; catalog number: 12604021) for iCMs and then counted with trypan blue solution (Thermofisher Scientific; catalog number: 15250061). The cells were then mixed accordingly based on the chosen cellular ratio of 2:1:1 (iCMs:HCF: HCAEC), which has proven effective in mimicking the human heart's microenvironment and were centrifuged at 300 g for 5 min. The cell pellet was resuspended in 190 $\mu$l of CS media, which is made up of iCMs media: HCF media: HCAEC media (2:1:1, respectively) and was plated in molten agarose 3D Petri dishes (81 wells) (figure 1(I)). Prior to that, the 3D Petri dishes were cast using micro-mold 3D Petri Dish® Microtissues® (Sigma-Aldrich, catalog number: Z764027), following the manufacturer's guidelines using 2% agarose (Sigma-Aldrich, catalog number: A4718) and diluted in phosphate-buffered saline (PBS) (Sigma-Aldrich, catalog number: D8537). To equilibrate the 3D Petri dishes, they were submerged in cell culture medium and left in the incubator (37 °C, 5%$O_2$, 5%$CO_2$) overnight before use. Each CS contained 30 000 cells and was generated by co-culturing 15 000 iCMs (three days post-thaw) with 7500 HCF and 7500 HCAEC, the co-culture medium, a blend tailored to the cellular components, facilitated spheroid formation within three days, with media replacements every two days (figure 1(II)).

To evaluate the impact of ACh-producing CNs, iCMs, HCAEC and HCF were co-cultured with Quick-Neuron Cholinergic-Human iPSC-derived Neurons (F, 74 yr donor) (Elixirgen Scientific, catalog number: CHSeV-CW50065-S) to form CNs. According to the manufacturer protocol, CNs were plated in Maintenance Medium iN1(AP) for 3 d.

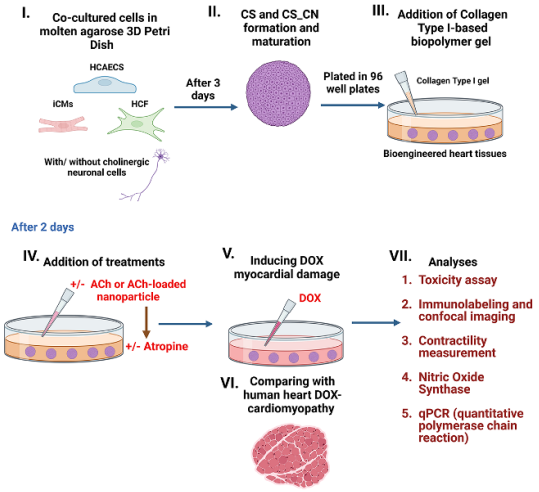


**Figure 1.** Schematic illustration of *in vitro* DOX-induced CS modeling. (I) Co-culture of human IPSC-derived cardiomyocytes (iCMs), human coronary artery endothelial cells (HCAEC), and human cardiac fibroblast (HCF) with or without CNs in a 3D petri dish. (II) Cardiac spheroids (CS) were formed and matured after three days. (III) CS are plated in collagen type I-biopolymer gel diluted with CS media in a 96-well plate. (IV) Acetylcholine (ACh) was added in some samples, as well as atropine, the antagonist of ACh. (V) Doxorubicin (DOX) was added to the samples and, after 24 h, underwent analyses. (VI) Human heart tissue cryosection was also used to compare with our DOX CS. (VII) The analyses are toxicity assay, immunolabeling and confocal imaging, contractile measurement and qPCR for *in vitro*, and nitric oxide synthase analysis for both *in vitro* and *ex vivo*.

Before thawing the cell line, the plate was coated overnight with laminin. According to previous studies, the ratio of the co-culture of neuronal cells to cardiomyocytes is 1:1 [43–45]. Overall, the ratio of 2 iCMs: 2 CNs: 1 HCF: 1 HCAEC for the culture, with the medium composition reflecting this ratio.

Upon reaching maturity after 3 d, both CS and CNs (figure 1(III)) were harvested and transferred to Falcon® 96-well Clear Microplates. These were embedded in a 100 $\mu$l collagen rat tail type 1 biopolymer gel (Merck, catalog number: 08-115) and mixed at a 1:1 ratio with additional media to adjust the gel's pH to 7.

### 2.3. ACh and atropine treatment

After 2 d, 100 $\mu$M ACh was added to CS (figure 1(IV)), with a concentration based on previous studies [46–48]. 50 $\mu$M atropine was added after 2h of administrating ACh as well as atropine was added to CNs after 2 d of being embedded in hydrogel. Atropine is an antagonist of ACh to understand the counter-effects of ACh.

### 2.4. Fabrication of ACh-NPs and PBCA-NPs

To prepare ACh-NPs, 10 mg of Polyvinylpyrrolidone (PVP) (Sigma-Aldrich, catalog number: PVP40T) was dissolved in 1 mL 10 mM citrate buffered solution of pH 3.5 to create a 1% w/v PVP solution. Subsequently, 10 mg of ACh was incorporated. Following this, 10 $\mu$l of PBCA (BRAUN, catalog number: 15054-BU) was injected into the mixture under continuous stirring to achieve a 1% v/v PBCA solution. The mixture was then allowed to stir for 30 min at room temperature and subsequently centrifuged at 20 000 g for 30 min. After centrifugation, the pellet was resuspended in PBS of pH 7.4 and filtered through a 1 $\mu$m PTFE syringe filter. The solution was dried using a SpeedVac (SpeedVac™ SPD121P) on an automated setting overnight for 12 h. The drying parameters were set as follows: a run temperature of 45 °C, heat time of 2.00 h, run time of 2.00 h, and a vacuum level of 14 Torr. For the control group involving PBCA-NPs, the same procedure was employed, excluding the addition of Acetylcholine chloride. The prepared nanoparticles were stored at 4 °C for a duration of up to one month.

#### *2.4.1. Calculation of entrapment efficiency*

Before transferring the NPs and spinning the solution, the weight of the empty tube (We) was noted. After the lyophilization step, the weight of respective tubes (Ws) was retaken (i.e., tube with lyophilized nanoparticles). The weight of NPs (Wn) is (Ws-We).

The PBCA-NPs are referred to as Wnc, and ACh-NPs as Wns. The formula for entrapment efficiency is as follows:

$$\text{Entrapment efficiency} = (\text{Wns} - \text{Wnc})/\text{Wnc} \times 100.$$

#### *2.4.2. Preparation of ACh-NPs and PBCA-NPs*

CS media was added to 1.70 mg mL$^{-1}$ for either ACh-NPs or PBCA-NPs and was sonicated for 12 min. Then, further diluted with media, 100µl of the solution was added per well at 0.17 mg mL$^{-1}$ (figure 1(IV)).

### 2.5. Addition of DOX

After 2 h of adding either ACh alone or together with atropine or ACh-NPs, 10 $\mu$m of DOX was added to the samples for 24 h (figure 1(V)). After that, the samples were analyzed through toxicity assay, immunolabelled cell types against cell death or eNOS, contractility assay, qPCR and stereo-seq analysis (figure 1(VII)).

### 2.6. Toxicity assay

The Live/Dead® Viability/Cytotoxicity Kit for mammalian cells (Invitrogen, catalog number: L32250) was employed following the instructions to evaluate cell viability, explicitly calculating the proportion of cells dead (stained with Ethidium Homodimer) relative to those alive (marked by Calcein-AM staining). In addition, NucBlue® Live ReadyProbes® Reagent (Hoechst 33342, Invitrogen, catalog number: R37605) was used as directed to determine the total cell population. 4 h after application; observations were made using a Leica Stellaris 8 confocal microscope (Leica Microsystems). Images were captured across three different fluorescent channels for each sample to determine the live, dead, and total cell counts. These images were analyzed using ImageJ software (Fiji), quantifying the fluorescence intensity of live versus dead cells, each compared to the total area. The viability metrics, calculated as the ratio of the dead-to-live cell, were initially compiled in Excel version 2401 (Microsoft 365) and subsequently analyzed using GraphPad Prism for detailed evaluation.

### 2.7. Tissue and CS immunolabeling and confocal imaging

To determine cell death for all cell types in CSs and CNs-CSs, the samples were stained with Ethidium Homodimer for at least 2 h then fixed with 10% neutral buffered, 4% (w/v) formaldehyde (Sigma-Aldrich, catalog number: HT5012) for 24 h. Afterward, the samples were washed in phosphate buffered saline/0.01% (w/v) sodium azide (0.01% (v/v) PBSA) three times for a period of 30 min and were permeabilized in 0.02% (v/v) Triton-X-100 (30 min). The samples were then blocked with 3% (v/v) bovine serum albumin (BSA)/PBSA solution (overnight). First antibody mouse monoclonal anti-human CD31 (1:10, diluted in 3% BSA/PBSA) was added to stain HCAEC and/or Anti-Choline Acetyltransferase (ChAT) (1:100, diluted in 3% BSA/PBSA) antibody to stain CNs overnight at 4 °C. The samples were then washed with 0.001% (v/v) PBSA three times and secondary antibody was added, Alexa fluor 647 goat anti-mouse (1:142, diluted in 3% BSA/PBSA) for

CS and/or Alexa Fluor 647 Goat Anti-Rabbit (1:142, diluted in 3% BSA/PBSA) and Alexa Fluor 790 Goat Anti-mouse (1:142, diluted in 3% BSA/PBSA) for CNs (overnight at 4 °C). The solution was removed, and the samples were washed three times with 0.001% (v/v) PBSA. NucBlue® Live ReadyProbes® Reagent (Hoechst 33342) was added for nuclei labeling in 3% BSA/PBSA with cTNT (1:10) to stain iCMs and Alexa Fluor® 488 vimentin (1:250) to stain HCF and the solution was left overnight at 4 °C. The samples were then washed with 0.001% (v/v) PBSA and stored at 4 °C.

To determine the concentration of eNOS level in human heart tissue samples (healthy, IHD, DOX cardiomyopathy and DCM) (figure 5(VI)), the frozen samples were cut at 50 $\mu$M at 20 °C using the NX70 cryostat (Leica Biosystems). We also evaluated the level of eNOS production in CS (media only, DOX and DOX ACh). All samples were fixed following the procedure above and stained with anti-phospho-eNOS/NOS III (Ser 114) antibody (15 $\mu$g $mL^{-1}$, rabbit immunoaffinity purified antibody) (Sigma-Aldrich; catalog number: 07-357) and Mouse Monoclonal anti-human CD31 overnight. After the three washes with 0.001% (v/v) PBSA, secondary antibodies were added following the conjugated antibodies and Hoechst.

All samples including cell death colocalized against all cell types and anti-phospho ENOS colocalized against all cell types were visualized using the Leica Stellaris 8 confocal microscope (Leica Microsystems). Optical sectioning along the $Z$-axis was performed, and the images collapsed into a single focal plane using the manufacturer's software, Microscope Software Platform LAS X Life Science (Leica Microsystems). The Z-stacks were processed using IMARIS software (Oxford Instruments plc, RRID:SCR_007370).

### 2.8. Fractional shortening and contractile frequency measurements

The contractile function of CS and CNs were analyzed using a Nikon Eclipse Ti2-E inverted microscope, and the contractility of each CS was recorded using the time frame option on NIS-Elements software. The fractional shortening percentage and the frequency of contractions are measured using Image J. This was done by measuring each sample's total number of contractions and the total length of each CS when contracted or relaxed.

### 2.9. mRNA isolation and quantitative polymerase chain reaction (qPCR) analysis

mRNA was extracted from the collected samples and analyzed through real-time polymerase chain reaction (qPCR) to measure changes in cardiovascular disease markers (angiogenesis, fibrosis, inflammation, cytoskeletal proteins, cell cycle-related proteins, apoptosis).

RNA isolation was carried out utilizing the guanidine-isothiocyanate lysis technique with the aid of the RNeasy Mini Kit (Qiagen, catalog number: 74104). Initially, samples underwent lysis and homogenization in the presence of absolute ethanol (100% v/v) to ensure optimal conditions for RNA binding. Subsequently, the lysates were applied to a RNeasy silica membrane for purification. The concentration and purity of the isolated total RNA were determined based on the absorbance ratio at 260 nm to 280 nm (A260/280), measured in a 10 mM Tris-Cl solution, pH 7.5. After quantification, each sample's total RNA was reverse transcribed into complementary DNA (cDNA) using the $RT^2$ First Strand Kit (Qiagen, catalog number: 330411). The resultant cDNA was then diluted appropriately for subsequent analyses using the $RT^2$ SYBR Green qPCR Master Mix (Qiagen, catalog number: 330503).

The qPCR assays were conducted on the Quantstudio 12 K Flex Real-Time PCR System (Thermo Fisher Scientific), employing the RT2 Profiler PCR Arrays (Qiagen, catalog number: 330231), which are designed to target mRNAs associated with human cardiovascular diseases specifically. Data analysis was performed using Qiagen's web-based software, applying the fold-change ($\Delta\Delta$Ct) method for quantitative assessment ($N = 3$).

### 2.10. Nitric oxide (NO) synthesis

Intracellular NO was detected using 1 $\mu$M DAF-FM diacetate solution (Sigma-Aldrich; catalog number: D2321) as previously described [6] Briefly, CS were treated with or without L-NIO (100 $\mu$M, Sigma-Aldrich; catalog number: 400600) for 60 min after two days of being plated in collagen gel. Then DOX, ACh and DOX + ACh were added and left in for two hours. The samples were rinsed twice with PBS, and 1 $\mu$M DAF-FM DA solution was freshly prepared in DMEM media with no phenol red (Thermo Fisher Scientific; catalog number: 21063029). After two hours, DAF-FM diacetate solution was removed, and the samples were rinsed twice with PBS, and fresh media was added. The samples were imaged using Leica Stellaris 8 confocal microscope (Leica Microsystems). Optical sectioning along the $Z$-axis was performed, and the images were collapsed into a single focal plane using Image J software (maximum intensity). NO synthesis was calculated by normalizing measurements against a total number of cells and then against all samples with Image J and analyzed using GraphPad Prism™ (La Jolla, CA).

### 2.11. Statistical analysis

*Data were analyzed using GraphPad Prism software to calculate mean ± SEM, and a one-way ANOVA test (Turkey multiple comparisons) or t-test were used to compare every sample. Significance was set to $p < 0.05$. For gene expression for the qPCR analysis, fold changes*

*were calculated as 2^(-Avg.ΔΔCt) and analyzed based on Qiagen web-based software.*

## 3. Results

### 3.1. Addition of ACh protects against DOX-induced toxicity and reduction in contractile activity

To evaluate the cardioprotective effects of ACh against DOX-induced toxicity, we added freely-suspended 100 $\mu$M ACh to DOX-treated for 24 h. We measured the toxicity ratio (dead/live cells) in CSs by staining dead cells with ethidium homodimer and live cells with calcein-AM. As shown in figures 2(A) and (B), the addition of ACh significantly reduced cell death and increased cell viability in DOX-treated CSs, while atropine (an ACh antagonist) counteracted ACh's protective effects.

Subsequently, we colocalized ethidium homodimer as a marker of cell death with cell-specific markers to identify cell-specific responses to ACh cardioprotection using IMARIS 3D rendering software. Our findings showed that ACh significantly attenuated DOX-induced death of cardiomyocytes (figure 2(C)), endothelial cells (figure 2(D)) and cardiac fibroblast (figure 2(E)). The addition of atropine counteracted ACh's effect, resulting in a significant increase in cardiomyocyte cell death in DOX-treated CSs, with no significant changes in cardiac endothelial cells and fibroblasts.

To evaluate any effects of ACh on DOX-induced reduction in CS contractile activity, we measured their contraction frequency and fractional shortening % (FS%) [8]. Our results showed that ACh protected against DOX-induced reduction in FS% while the addition of atropine counteracted ACh's protective effects (figure 2(H)). ACh did not significantly improve contraction frequency in DOX-treated CSs (figure 2(G)). To identify the mechanisms regulating ACh cardioprotection, we performed qPCR analyses of genes regulating cardiovascular pathophysiology (supplementary table 1). ACh significantly reversed DIC-induced upregulation of cardiac remodeling genes, such as matrix metallopeptidase 13 and renin (REN), indicative of extracellular matrix (ECM) protein degradation. Additionally, ACh reduced the DOX-induced increase of SNCA (alpha-synuclein) mRNA levels, which regulates apoptosis. The addition of ACh to DOX-treated CSs also increased phosphodiesterase 5A (PDE5A), which controls the $\beta$-adrenergic system.

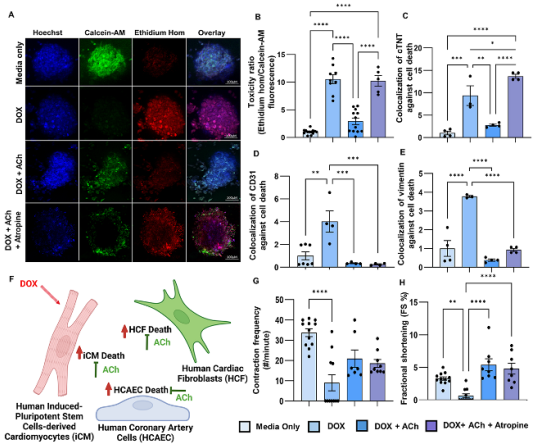


**Figure 2.** Protective role of addition of ACh against DOX CS. (A) Confocal stack images of CSs treated as follows: (*i*) media only (control); (*ii*) 10 $\mu$M DOX; (*iii*) 10 $\mu$M DOX + 100 $\mu$M ACh; and (*iv*) 10 $\mu$M DOX + 100 $\mu$M ACh + 50 $\mu$M atropine. CSs were stained with Hoechst (blue, nuclei), calcein-AM (green, live cells) and ethidium homodimer (red, dead cells). The magnification bars equal 100 $\mu$m. (B) Toxicity ratio (dead cells/ live cells, normalized against control); $N \geqslant 5$. (C) Colocalization of cTNT-positive cells (iCMs) and cell death (ethidium homodimer) in CSs; $N \geqslant 3$. (D) Colocalization of CD31-positive cells (HCAECs) and cell death (ethidium homodimer) in CSs; $N \geqslant 3$. (E) Colocalization of vimentin-positive cells (HCFs) and cell death (ethidium homodimer) in CSs; $N \geqslant 3$. (F) Schematic illustration of the protective effects of ACh against DOX based on the colocalization measurements in (C)–(E). (G) Fractional shortening % (FS%) in CSs; $N > 7$. (H) Contraction frequency of CS; $N > 7$. (B)–(E) and (G), (H) Each individual point in the figures corresponds to a replicate of a single CS and mean ± SEM, with error bars indicating the standard error of the mean. Statistical significance is denoted as $P < 0.05 = *$, $p < 0.01 = **$, $p < 0.001 = ***$ and $p < 0.0001 = ****$, analyzed using One-way ANOVA followed by Tukey's multiple comparisons tests (normalized against control except for (G) and (H)).

### 3.2. Cholinergic neurons (CNs) protect against DOX-induced toxicity and reduction in contractile activity

We next sought to elucidate the cardioprotective role of ACh-derived from cholinergic nerves against DOX by co-culturing CNs with CSs (CN-CSs). As illustrated in figure 3(A), viable cells stained with calcein-AM and dead cells stained with ethidium homodimer either in the presence or absence of DOX when CNs were added to CSs. These observations were confirmed by our statistical analysis of the toxicity ratios (figure 3(B)). Atropine significantly increased the toxicity ratios in DOX-treated CSs (figures 3(A) and (B)), supporting an ACh-dependent protective effect. After the colocalization of ethidium homodimer (cell death marker) with cell-specific markers in CN-CSs, we measured no significant changes in cell death for cardiomyocytes (figure 3(C)), endothelial cells (figure 3(D)), fibroblasts (figure 3(E)), and CNs (figure 3(F)) following DOX treatment. On the contrary, atropine increased DOX-induced toxicity in CN-CSs specifically in endothelial cells (figure 3(D)).

The addition of CNs to DOX-treated CSs also prevented any changes in contraction frequency (figure 3(G)) and FS% (figure 3(H)), while atropine significantly reduced contractile activity in CN-CSs (figures 3(g) and (H)).

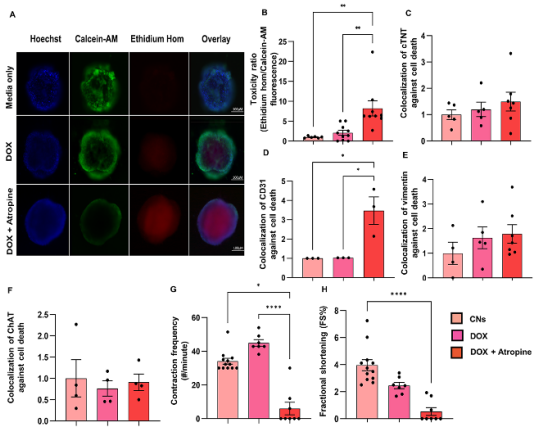


**Figure 3.** Protective role of ACh-producing CNs against DIC in CN-CSs. (A) Epifluorescence stack images of CN-CSs treated as follows; (*i*) media only (control); (*ii*) 10 $\mu$M DOX; (*iii*) 10 $\mu$M DOX + 50 $\mu$M atropine. CN-CSs were stained with Hoechst (blue, nuclei), calcein-AM (green, live cells) and ethidium homodimer (red, dead cells). The magnification bars equal 100 $\mu$m. (B) Toxicity ratio (dead cells/ live cells, normalized against control); $N \geqslant 6$. (C) Colocalization of cTNT-positive cells (iCMs) and cell death (ethidium homodimer) in CN-CSs; $N \geqslant 4$. (D) Colocalization of CD31-positive cells (HCAECs) and cell death (ethidium homodimer) in CN-CSs; $N = 3$. (E) Colocalization of vimentin-positive cells (HCFs) and cell death (ethidium homodimer) in CN-CSs; $N \geqslant 4$. (F) Colocalization of ChAT expression in CNs and cell death (ethidium homodimer) in CN-CSs; $N = 4$. (G) Contraction Frequency of CN-CSs; $N \geqslant 7$. (H) FS% analysis of CN-CSs; $N \geqslant 7$. (B)–(H) Each individual point in the figures corresponds to a replicate of a single CS and mean ± SEM, with error bars indicating the standard error of the mean. Statistical significance is denoted as $P < 0.05 = *$, $p < 0.01 = **$, $p < 0.001 = ***$ and $p < 0.0001 = ****$, analyzed using One-way ANOVA followed by Tukey's multiple comparisons tests (normalized against control except for (G) and (H)).

When we measured changes in gene expression levels, monoamine oxidase-A (MAOA) was significantly increased in DOX-treated CN-CSs compared to CN-CSs (supplementary table 2). MAO controls the breakdown of other neurotransmitters, such as serotonin, epinephrine, norepinephrine, and dopamine. Following the addition of DOX to CN-CSs, we also measured an upregulation in adrenergic receptors ADRA1A and ADRA1D, which regulate catecholamines, norepinephrine and epinephrine signaling. DOX also upregulated phosphodiesterase 3B, which regulates lipolysis, energy homeostasis and insulin secretion, in CN-CSs.

### 3.3. ACh-NPs protect against DOX-induced cell death and reduction in contraction function

Given the fact that ACh hydrolyses rapidly and higher doses might be used to achieve the desired biological response, there is a high chance that systemic ACh administration could lead to undesired side effects, including lacrimation, salivation, tremors, loss of motor activity, hypothermia, and tonic convulsions [49]. To deliver ACh in a targeted manner and prevent its potential side effects in other tissues and organs while also reducing its dose, we generated a novel therapeutic approach for ACh delivery in combination with PBCA-NPs. ACh-NPs were created by loading ACh in PBCA-NPs, with a loading efficacy of 17.50% (supplementary figure S1 and supplementary table S3). Further characterization of ACh-NPs was performed, and the results from 3 biological and technical replicates showed that the size of ACh-NPs was 108.304 nm ± 6.805, the polydispersity index was 0.117 ± 0.052 and the Z-potential was 4.754 mV ± 0.955 (supplementary table S4).

As indicated in figures 4(A) and (B), ACh-NPs significantly mitigated DOX-induced toxicity in CSs, while control PBCA-NPs (which did not contain any ACh) had no significant protective effects. After our colocalization of DOX-treated CSs with ethidium homodimer (cell death) and antibodies against the three cell types, we found that ACh-NPs significantly attenuated cell death in endothelial cells (figure 4(D)) and fibroblasts (figure 4(E)), while this effect was not statistically significant in cardiomyocytes (figure 4(C)). The protection provided by ACh-NPs against cell death was supported by similar effects on contractile frequency and FS% (figures 4(f) and (G)). Although we demonstrated significant effects of ACh-NPs compared to DOX, we did not include DOX + PBCA-NPs as a control group for figures 4(C)–(G) due to limitations in resources and funding.

### 3.4. ACh inhibits phospho-eNOS expression in endothelial cells of DOX-treated CSs

We previously identified NO through the activation of eNOS signaling as a major regulator of DOX-induced toxicity in endothelial cells and fibroblasts in CSs [6] Therefore, we investigated whether ACh could inhibit NO signaling following DOX treatment in CS (figure 5(A)). We, therefore, measured any changes in intracellular NO production using DAF-FM, which becomes fluorescent in the presence of NO within cells. ACh did not significantly decrease the overall NO in CSs (supplementary figure S2). However, after colocalizing antibodies against activated eNOS (phospho-eNOS) and antibodies staining cell-specific markers, ACh significantly inhibited eNOS activation in endothelial cells (figures 5(B)–(E)), suggesting that ACh protection against DOX toxicity in CSs is dependent on NO signaling within endothelial cells. This is consistent with previous findings highlighting a dual role of NO in being both cardioprotective at homeostasis and cardiotoxic when exacerbated to high levels, especially in the generation of peroxynitrite [6].

To potentially translate our *in vitro* findings to human heart samples, we stained human heart biopsies from the Sydney Heart Biobank with antibodies against phospho-eNOS and antibodies against the markers of the three cell types in CSs (supplementary figure S3). Consistent with our

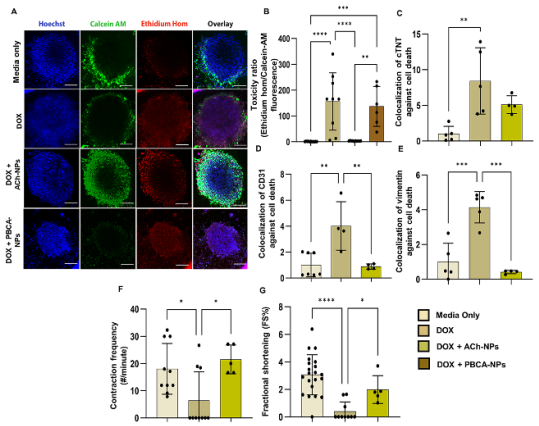


**Figure 4.** Protective role of ACh-NPs against DOX CS. (A) Confocal stack images of CSs treated as follows: (*i*) media only (control); (*ii*) 10 $\mu$M DOX; (*iii*) 10 $\mu$M DOX + ACh-NPs; and (*iv*) 10 $\mu$M DOX + PBCA-NPs. CSs were stained with Hoechst (blue, nuclei), calcein-AM (green, live cells) and ethidium homodimer (red, dead cells). The magnification bars equal 100 $\mu$m. (B) Toxicity ratio (dead cells/ live cells, normalized against control); $N \geqslant 7$. (C) Colocalization of cTNT-positive cells (iCMs) and cell death (ethidium homodimer) in CSs; $N \geqslant 4$. (D) Colocalization of CD31-positive cells (HCAECs) and cell death (ethidium homodimer) in CSs; $N \geqslant 4$. (E) Colocalization of vimentin-positive cells (HCFs) and cell death (ethidium homodimer) in CSs; $N \geqslant 4$. (F) FS% in CSs; $N \geqslant 5$. (G) Contraction Frequency in CSs; $N \geqslant 5$. (B)–(G) Each individual point in the figures corresponds to a replicate of a single CS and mean ± SEM, with error bars indicating the standard error of the mean. Statistical significance is denoted as $P < 0.05 = *$, $p < 0.01 = **$, $p < 0.001 = ***$ and $p < 0.0001 = ****$, analyzed using One-way ANOVA followed by Tukey's multiple comparisons tests (normalized against control except for (F) and (G)).

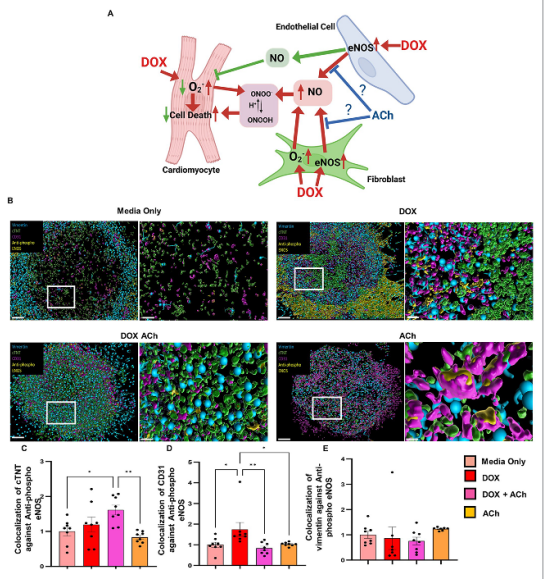


**Figure 5.** Effect of ACh on nitric oxide synthase through eNOS pathway. (A) Schematic illustration of DOX-induced cell death in CSs dependent on eNOS signaling and potential ACh-mediated protection in endothelial cells and fibroblasts via eNOS inhibition. (B) 3D rendering images of the three cell types of CS against ENOS. Samples are as follows: (*i*) media only (control); (*ii*) 10 $\mu$M DOX; (*iii*) 10 $\mu$M DOX + 100 $\mu$M ACh; and (*iv*) 100 $\mu$M ACh. CSs were stained with vimentin (cyan, HCF), cTNT (green, iCMs), CD31 (magenta, HCAECs), and anti-phospho eNOS (yellow, eNOS) in CS. Magnification bars are 100 $\mu$m and 20 $\mu$m. (C) Colocalization of cTNT against anti-phospho ENOS in CS; $N \geqslant 9$. (D) Colocalization of CD31 against anti-phospho ENOS in CS; $N \geqslant 7$. (E) Colocalization of vimentin against anti-phospho ENOS in CS; $N \geqslant 6$. (C)–(E) Data are presented as individual points and mean ± SEM, with error bars indicating the standard error of the mean. Statistical significance is denoted as $P < 0.05 = *$, $p < 0.01 = **$, $p < 0.001 = ***$ and $p < 0.0001 = ****$, analyzed using One-way ANOVA followed by Tukey's multiple comparisons test (normalized against control).

*in vitro* results in CSs, DOX significantly increased phospho-eNOS expression in endothelial cells in human heart tissues (supplementary figure S3(C)). Altogether, our *in vitro* and *ex vivo* findings support that ACh is cardioprotective against DOX by inhibiting eNOS signaling in endothelial cells.

## 4. Discussion

Previous studies showed that ACh is protective against cardiovascular disease [18, 22, 24, 50], Alzheimer's disease [51–53] and dementia [54, 55]. Increasing ACh levels through vagus nerve stimulation (VNS) and cholinesterase inhibitors, such as donepezil, are cardioprotective against DIC by improving mitochondrial function, reducing cardiomyocyte apoptosis and improving left ventricles function in rat models [3, 27–29]. However, VNS is an invasive surgical procedure [56], and cholinesterase inhibitors lead to adverse drug reactions, including tiredness, panic, sweating, diarrhea, vomiting, muscle tension, speech difficulty, and involuntary tremors [57]. VNS protects against endothelial dysfunction [58] and prevented contractile dysfunction in DOX-induced rat models [50, 59]. However, clinical trials using ACh and VNS have shown mixed results, mostly due to the lack of a systematic approach in the experimental plan [34]. We have previously shown that CSs can be used to study DOX-induced toxicity and potentially prevent its toxic effects by inhibiting downstream signaling pathways by using either pharmacological or genetic inhibition [6]. In this study, we demonstrated that the addition of ACh through the three delivery methods reduced total cell death (figures 2–4). However, ACh-NPs predominantly reduced cell death in endothelial cells and fibroblasts (figure 4), which is consistent with our previous findings in CSs [6], where eNOS signaling inhibition reduced DOX-induced toxicity. Additionally, ACh-NPs also protected against the reduction in contraction frequency and FS% (figure 3).

Our results in CSs on DOX-dependent eNOS signaling in endothelial cells are consistent with the ones in *ex vivo* DOX-treated biopsies (figure 5 and supplementary figure S3). It is only with the use of *in vitro* CSs that we were then able to show that ACh reduced eNOS activation in endothelial cells following DOX treatment [6], which was associated with improved

viability and contractile function (figure 2). Our findings are consistent with previous studies. At physiological concentrations, NO plays a protective role in the heart when synthesized by eNOS in both cardiomyocytes and endothelial cells [60]. NO release from vascular eNOS regulates myocyte relaxation, diastolic function and vascular function [61–63]. It also plays a crucial role in cardiomyocyte functions, such as ion channel regulation, contractility, $Ca^{2+}$ homeostasis, cell growth and survival [64]. Nevertheless, excessive eNOS activation in endothelial cells can trigger DOX-induced toxicity in cardiomyocytes [6]. Kalivendi *et al* [65] demonstrated that inhibiting eNOS in endothelial cells attenuated DOX-induced ROS production and apoptosis. Kuwabara *et al* [66] reported that increasing ACh in cardiomyocytes during hypoxia led to an increase in NO production, which activated the production of vascular endothelial growth factor and accelerated angiogenesis [66]. Oikawa *et al* [5] showed that knocking down a heart-specific choline acetyltransferase (ChAT) leads to a significant decrease in NO production in cardiomyocytes and cardiac dysfunction in mice.

Our results also suggested that ACh protected CSs against DIC by inhibiting ECM protein degradation, myocardial fibrosis and cardiac remodeling through MMP-13 (supplementary table 1). DOX upregulates MMP-13 expression, which is also a typical feature of vascular disease, myocardial fibrosis and cardiac remodeling [67–70]. Furthermore, the administration of ACh reduced the overexpression of the SNCA (supplementary table 1), which is a common biomarker for Parkinson's disease and is highly expressed in patients with stroke or atrial fibrillation, impairing the autonomic system by increasing norepinephrine levels and inhibiting ACh-induced relaxation [71]. Studies have also shown that DIC causes a shift in the autonomic balance toward sympathetic predominance [27, 72] and has an atropine-like inhibitory effect on cardiac ACh receptor signaling, drastically reducing cardiac contractility and heart rate [3, 73]. Our results demonstrated that increasing ACh in DOX-treated CSs led to the upregulation of PDE5A expression (supplementary table 1), which activates $\beta$-adrenergic receptors and is responsible for pressure overload in the heart [74, 75]. We also measured an upregulation of MAOA and adrenergic receptors, including ADRA1A and ADRA1B, in ACh-derived CNs exposed to DIC (supplementary table 2). These genes are associated with the sympathetic nervous pathway, and the elevation of catecholamines, epinephrine, and norepinephrine are hallmarks of many cardiovascular disorders [76]. Moreover, emerging evidence suggests that ADRA1A could provide cytoprotective effects by enhancing contractility [77] and activating glucose intake [78] in cardiomyocytes.

In this study, we demonstrated for the first time a novel therapeutic approach using ACh-NPs that has shown to be promising in improving contractile function and reducing necrotic death in endothelial cells and fibroblasts against DOX-induced CSs (figure 4(A)). To ensure specificity to ACh in any effects of ACh-NPs in CSs and not to the PBCA-NPs themselves, we also tested the effects of PBCA-NPs (without any ACh), as a negative control [79]. Our findings indicated that PBCA-NPs had no effects (figure 4(A)). However, further studies are required to explore the protective role of ACh-NPs specifically in cardiomyocytes and their long-term effects. Future work should also revolve around the efficacy and delivery of ACh-NPs including improving their stability, targeting efficiency, and controlled release properties, which is necessary. Comparative studies with *in vivo* models using murine or pig model are also necessary to validate our findings from the CS model and establish their relevance to human cardiac physiology and disease.

One limitation of our study is that while we have demonstrated the potential protective effects of ACh against DOX, we have yet to quantify the final concentration of freely-dissolved ACh and ACh-NPs within CSs. Future studies will incorporate the use of a choline/acetylcholine quantification kit to measure ACh levels accurately. Additionally, to better understand ACh-NPs' delivery mechanism and optimize therapeutic strategies, we will investigate the localization of ACh-NPs within CSs.

Another critical consideration is the potential variability in the response of CS models compared to *in vivo* conditions. Although CSs effectively mimic human heart tissue pathophysiology, they lack certain features that are dependent on blood flow and multi-organ responses. Future studies on DOX-induced toxicity could address these limitations by incorporating other cell types, such as inflammatory, immune, and sympathetic neuron cells, as well as dynamic conditions like blood flow and paracrine effects. Such an approach would provide a more comprehensive understanding of DOX-induced toxicity mechanisms. Additionally, evaluating DOX-induced toxicity in both heart and cancer tissues could help determine the optimal dosage of DOX in conjunction with the cardioprotective effects of ACh-NPs.

Other limitations include the timing of ACh-NPs administration. In our study, ACh-NPs were administered prior to DOX-induced myocardial damage in CSs, whereas cardiotoxicity in cancer patients often manifests years after DOX treatment, sometimes up to 17 years later [80]. This underscores the importance of investigating the timing of ACh-NPs delivery to patients. Administering ACh-NPs before DOX treatment might prevent chronic myocardial damage,

but further studies are needed to confirm this. It will also be critical to determine the most effective delivery method for ACh-NPs, whether intravenously or orally.

Lastly, while our *in vitro* models have demonstrated promising results, translating these findings to clinical settings remains a challenge. The complexity of human CVD may not be fully replicated in animal models, and species-specific and sex-specific differences in response to ACh treatments must be considered. Future research should include *in vivo* experimentation in both small and large animal models, such as pigs, which possess cardiac functions comparable to humans. [79] These efforts will be essential to bridging the gap between preclinical studies and clinical applications.

## 5. Conclusion

In conclusion, our study highlights the potential of increasing ACh levels as a therapeutic strategy against DIC and underscores the utility of the CS model in advancing our understanding of cardiac protection mechanisms. Our findings support the protective role played by ACh against DOX-induced toxicity, necrosis, reduction in contractile function and progression to HF. We also showed for the first time that ACh-NPs could be a promising therapeutic approach to attenuate DOX-induced cell death in endothelial cells and fibroblasts and prevent contractile dysfunction. However, additional studies are required to evaluate the optimal dosage of ACh-NPs delivery and to translate our *in vitro* findings to *in vivo* studies.

## Data availability statement

The data that support the findings of this study are openly available at the following URL/DOI: https://osf.io/nd5ja/.

## Acknowledgment

We thank Associate Professor Louise Cole and Dr Amy Bottomley (Microbial Imaging Facility, UTS) for microscopy assistance. We thank the staff and patients of St. Vincent's Hospital Sydney and the Australian Red Cross Blood Service. CG was supported by a UTS Seed Funding and Catholic Archdiocese of Sydney Grant for Adult Stem Cell Research, a Heart Research Institute Fellowship, Heart Research Australia, a 2023 and a 2024 Perpetual IMPACT Grants and a Ian Potter Foundation Medical Research Grant. XW was supported by the National Heart Foundation Future Leader Fellowship and Baker Fellowship. CLCM was supported by NSW Waratah Scholarship. SL was supported by the RT Hall Trust and the Baird Institute.

## ORCID iDs

Clara Liu Chung Ming https://orcid.org/0000-0001-9414-3499
Ahmed Refaat https://orcid.org/0000-0002-0353-4935
Carmine Gentile https://orcid.org/0000-0002-3689-4275

## References

[1] Volkova M and Russell R 2011 Anthracycline cardiotoxicity prevalence, pathogenesis and treatment *Curr. Cardiol. Rev.* **7** 214–20
[2] Christidi E and Brunham L R 2021 Regulated cell death pathways in doxorubicin-induced cardiotoxicity *Cell Death Dis.* **12** 339
[3] Prathumsap N *et al* 2022 Acetylcholine receptor agonists provide cardioprotection in doxorubicin-induced cardiotoxicity via modulating muscarinic M2 and α7 nicotinic receptor expression *Transl. Res.* **243** 33–51
[4] Abdel-Daim M M, Kilany O E, Khalifa H A and Ahmed A A M 2017 Allicin ameliorates doxorubicin-induced cardiotoxicity in rats via suppression of oxidative stress, inflammation and apoptosis *Cancer Chemother. Pharmacol.* **80** 745–53
[5] Oikawa S, Kai Y, Mano A, Ohata H, Kurabayashi A, Tsuda M and Kakinuma Y 2021 Non-neuronal cardiac acetylcholine system playing indispensable roles in cardiac homeostasis confers resiliency to the heart *J. Physiol. Sci.* **71** 2
[6] Polonchuk L, Chabria M, Badi L, Hoflack J-C, Figtree G, Davies M J and Gentile C 2017 Cardiac spheroids as promising *in vitro* models to study the human heart microenvironment *Sci. Rep.* **7** 1–12
[7] Octavia Y, Tocchetti C G, Gabrielson K L, Janssens S, Crijns H J and Moens A L 2012 Doxorubicin-induced cardiomyopathy From molecular mechanisms to therapeutic strategies *J. Mol. Cell Cardiol.* **52** 1213–25
[8] Sharma P, Ming C L C, Wang X, Bienvenu L A, Beck D, Figtree G A, Boyle A and Gentile C 2022 Biofabrication of advanced *in vitro* 3D models to study ischaemic and doxorubicin-induced myocardial damage *Biofabrication* **14** 025003
[9] Cavalcante G L, Brognara F, Oliveira L, Lataro R M, Durand M, de Oliveira A P, da Nóbrega A C L, Salgado H C and Sabino J P J 2021 Benefits of pharmacological and electrical cholinergic stimulation in hypertension and heart failure *Acta Physiol.* **232** e13663
[10] Elamin A B A, Forsat K, Senok S S and Goswami N 2023 Vagus nerve stimulation and its cardioprotective abilities a systematic review *J. Clin. Med.* **12** 1717
[11] Hadaya J and Ardell J L 2020 Autonomic modulation for cardiovascular disease *Front. Physiol.* **11** 617459
[12] Mahmoud A I *et al* 2015 Nerves regulate cardiomyocyte proliferation and heart regeneration *Dev. Cell* **34** 387–99
[13] Intachai K, Chattipakorn S C, Chattipakorn N and Shinlapawittayatorn K 2018 Revisiting the cardioprotective effects of acetylcholine receptor activation against myocardial ischemia/reperfusion injury *Int. J. Mol. Sci.* **19** 2466
[14] Liu Chung Ming C, Wang X and Gentile C 2024 Protective role of acetylcholine and the cholinergic system in the injured heart *iScience* **27** 110726
[15] Kalay N *et al* 2006 Protective effects of carvedilol against anthracycline-induced cardiomyopathy *J. Am. Coll. Cardiol.* **48** 2258–62
[16] Bezerra O C *et al* 2017 Cholinergic stimulation improves oxidative stress and inflammation in experimental myocardial infarction *Sci. Rep.* **7** 13687

[17] Buchholz B, Donato M, Perez V, Ivalde F C, Höcht C, Buitrago E, Rodríguez M and Gelpi R J 2012 Preischemic efferent vagal stimulation increases the size of myocardial infarction in rabbits *role of the sympathetic nervous system Int. J. Cardiol.* **155** 490–1
[18] Intachai K, Chattipakorn S C, Chattipakorn N and Shinlapawittayatorn K 2022 Acetylcholine exerts cytoprotection against hypoxia/reoxygenation-induced apoptosis, autophagy and mitochondrial impairment through both muscarinic and nicotinic receptors *Apoptosis* **27** 233–45
[19] Kakinuma Y, Akiyama T, Okazaki K, Arikawa M, Noguchi T and Sato T 2012 A non-neuronal cardiac cholinergic system plays a protective role in myocardium salvage during ischemic insults *PLoS One* **7** e50761
[20] Kakinuma Y, Tsuda M, Okazaki K, Akiyama T, Arikawa M, Noguchi T and Sato T 2013 Heart-specific overexpression of choline acetyltransferase gene protects murine heart against ischemia through hypoxia-inducible factor-1α-related defense mechanisms *J. Am. Heart Assoc.* **2** e004887
[21] Katare R G, Ando M, Kakinuma Y, Arikawa M, Handa T, Yamasaki F and Sato T 2009 Vagal nerve stimulation prevents reperfusion injury through inhibition of opening of mitochondrial permeability transition pore independent of the bradycardiac effect *J. Thorac. Cardiovasc. Surg.* **137** 223–31
[22] Munasinghe P E, Saw E L, Reily-Bell M, Tonkin D, Kakinuma Y, Fronius M and Katare R 2023 Non-neuronal cholinergic system delays cardiac remodelling in type 1 diabetes *Heliyon* **9** e17434
[23] De Ferrari G M *et al* 2010 Chronic vagus nerve stimulation a new and promising therapeutic approach for chronic heart failure *Eur. Heart J.* **32** 847–55
[24] Gold M R *et al* 2016 Vagus nerve stimulation for the treatment of heart failure *J. Am. Coll. Cardiol.* **68** 149–58
[25] Borovikova L V, Ivanova S, Zhang M, Yang H, Botchkina G I, Watkins L R, Wang H, Abumrad N, Eaton J W and Tracey K J 2000 Vagus nerve stimulation attenuates the systemic inflammatory response to endotoxin *Nature* **405** 458–62
[26] Calvillo L, Vanoli E, Andreoli E, Besana A, Omodeo E, Gnecchi M, Zerbi P, Vago G, Busca G and Schwartz P J 2011 Vagal stimulation, through its nicotinic action, limits infarct size and the inflammatory response to myocardial ischemia and reperfusion *J. Cardiovasc. Pharmacol.* **58** 500–7
[27] Guo F *et al* 2022 Choline protects the heart from doxorubicin-induced cardiotoxicity through vagal activation and Nrf2/HO-1 pathway *Oxid. Med. Cell. Longev.* **2022** 4740931
[28] Siripakkaphant C, Ongnok B, Prathumsap N, Khuanjing T, Chunchai T, Arunsak B, Pantiya P, Chattipakorn N and Chattipakorn S C 2023 Vagus nerve stimulation provides neuroprotection against doxorubicin-induced chemobrain via activations of both muscarinic and nicotinic acetylcholine receptors *Alzheimer's Dementia* **19** e073548
[29] Khuanjing T, Ongnok B, Maneechote C, Siri-Angkul N, Prathumsap N, Arinno A, Chunchai T, Arunsak B, Chattipakorn S C and Chattipakorn N 2021 Acetylcholinesterase inhibitor ameliorates doxorubicin-induced cardiotoxicity through reducing RIP1-mediated necroptosis *Pharmacol. Res.* **173** 105882
[30] Liu Chung Ming C, Sesperez K, Ben-Sefer E, Arpon D, McGrath K, McClements L and Gentile C 2021 Considerations to model heart disease in women with preeclampsia and cardiovascular disease *Cells* **10** 899
[31] Liu Chung Ming C, Ben-Sefer E and Gentile C 2022 Stem cell-based 3D bioprinting for cardiovascular tissue regeneration *Advanced Technologies in Cardiovascular Bioengineering* (Springer) pp 281–312
[32] Chung Ming C L *et al* 20243D in vitro modelling of post-partum cardiovascular health reveals unique characteristics and signatures following hypertensive disorders in pregnancy *Biol Sex Differ* **15** 94
[33] Kröger E, Mouls M, Wilchesky M, Berkers M, Carmichael P-H, van Marum R, Souverein P, Egberts T and Laroche M-L 2015 Adverse drug reactions reported with cholinesterase inhibitors an analysis of 16 years of individual case safety reports from VigiBase *Ann. Pharmacother.* **49** 1197–206
[34] Zafeiropoulos S, Ahmed U, Bikou A, Mughrabi I T, Stavrakis S and Zanos S 2023 Vagus nerve stimulation for cardiovascular diseases Is there light at the end of the tunnel? *Trends Cardiovasc. Med.* **34** 327–37
[35] Evangelatov A, Skrobanska R, Mladenov N, Petkova M, Yordanov G and Pankov R 2016 Epirubicin loading in poly (butyl cyanoacrylate) nanoparticles manifests via altered intracellular localization and cellular response in cervical carcinoma (HeLa) cells *Drug Deliv.* **23** 2235–44
[36] Sulheim E, Baghirov H, von Haartman E, Bøe A, Åslund A K, Mørch Y and Davies Cd L 2016 Cellular uptake and intracellular degradation of poly (alkyl cyanoacrylate) nanoparticles *J. Nanobiotechno.* **14** 1–14
[37] Refaat A, Del Rosal B, Bongcaron V, Walsh A P G, Pietersz G, Peter K, Moulton S E and Wang X 2023 Activated platelet-targeted IR780 immunoliposomes for photothermal thrombolysis *Adv. Funct. Mater.* **33** 2209019
[38] Rempe R, Cramer S, Hüwel S and Galla H-J 2011 Transport of Poly(n-butylcyano-acrylate) nanoparticles across the blood–brain barrier *in vitro* and their influence on barrier integrity *Biochem. Biophys. Res. Commun.* **406** 64–69
[39] Reukov V, Maximov V and Vertegel A 2011 Proteins conjugated to poly(butyl cyanoacrylate) nanoparticles as potential neuroprotective agents *Biotechnol. Bioeng.* **108** 243–52
[40] Wang C, Jiang H, Zhu J and Jin Y 2024 A new agent for contrast-enhanced intravascular ultrasound imaging *in vitro* polybutylcyanoacrylate nanoparticles with drug-carrying capacity *Artif. Cells Nanomed. Biotechnol.* **52** 218–28
[41] Figtree G A, Bubb K J, Tang O, Kizana E and Gentile C 2017 Vascularized cardiac spheroids as novel 3D *in vitro* models to study cardiac fibrosis *Cells Tissues Organs* **204** 191–8
[42] Sharma P, Ming C L C and Gentile C 2022 *In vitro* modeling of myocardial ischemia/reperfusion injury with murine or human 3D cardiac spheroids *STAR Protocols* **3** 101751
[43] Takayama Y and Kida Y S 2016 *In vitro* reconstruction of neuronal networks derived from human iPS cells using microfabricated devices *PLoS One* **11** e0148559
[44] Mukae Y, Itoh M, Noguchi R, Furukawa K, Arai K, Oyama J, Toda S, Nakayama K, Node K and Morita S 2018 The addition of human iPS cell-derived neural progenitors changes the contraction of human iPS cell-derived cardiac spheroids *Tissue Cell* **53** 61–67
[45] Sakai K, Shimba K, Ishizuka K, Yang Z, Oiwa K, Takeuchi A, Kotani K and Jimbo Y 2017 Functional innervation of human induced pluripotent stem cell-derived cardiomyocytes by co-culture with sympathetic neurons developed using a microtunnel technique *Biochem. Biophys. Res. Commun.* **494** 138–43
[46] Krieg T, Qin Q, Philipp S, Alexeyev M F, Cohen M V and Downey J M 2004 Acetylcholine and bradykinin trigger preconditioning in the heart through a pathway that includes Akt and NOS *Am. J. Physiol. Heart Circ. Physiol.* **287** H2606–H11
[47] Rana O R *et al* 2010 Acetylcholine as an age-dependent non-neuronal source in the heart *Auton. Neurosci.* **156** 82–89
[48] Roy A, Dakroub M, Tezini G C, Liu Y, Guatimosim S, Feng Q, Salgado H C, Prado V F, Prado M A M and Gros R 2016 Cardiac acetylcholine inhibits ventricular remodeling and dysfunction under pathologic conditions *FASEB J.* **30** 688–701
[49] Broomfield C A, Maxwell D, Solana R, Castro C, Finger A and Lenz D 1991 Protection by butyrylcholinesterase against organophosphorus poisoning in nonhuman primates *J. Pharmacol. Exp. Ther.* **259** 633–8
[50] Nuntaphum W, Pongkan W, Wongjaikam S, Thummasorn S, Tanajak P, Khamseekaew J, Intachai K, Chattipakorn S C,

Chattipakorn N and Shinlapawittayatorn K 2018 Vagus nerve stimulation exerts cardioprotection against myocardial ischemia/reperfusion injury predominantly through its efferent vagal fibers *Basic Res. Cardiol.* **113** 22
[51] Bordier P, Garrigue S, Lanusse S, Margaine J, Robert F, Gencel L and Lafitte A 2006 Cardiovascular effects and risk of syncope related to donepezil in patients with Alzheimer's disease *CNS Drugs* **20** 411–7
[52] Ongnok B, Khuanjing T, Chunchai T, Kerdphoo S, Jaiwongkam T, Chattipakorn N and Chattipakorn S C 2021 Donepezil provides neuroprotective effects against brain injury and Alzheimer's pathology under conditions of cardiac ischemia/reperfusion injury *Biochim. Biophys. Acta* **1867** 165975
[53] Pu Z, Xu W, Lin Y, Shen J and Sun Y 2019 Donepezil decreases heart rate in elderly patients with Alzheimer's disease *Int. J. Clin. Pharmacol. Ther.* **57** 94
[54] Battle C E, Abdul-Rahim A H, Shenkin S D, Hewitt J and Quinn T J 2021 Cholinesterase inhibitors for vascular dementia and other vascular cognitive impairments a network meta-analysis *Cochrane Database Syst. Rev.* CD013306
[55] Jian W-X, Zhang Z, Zhan J-H, Chu S-F, Peng Y, Zhao M, Wang Q and Chen N-H 2020 Donepezil attenuates vascular dementia in rats through increasing BDNF induced by reducing HDAC6 nuclear translocation *Acta Pharmacol. Sin.* **41** 588–98
[56] Choudhary R C *et al* 2022 Threshold adjusted vagus nerve stimulation after asphyxial cardiac arrest results in neuroprotection and improved survival *Bioelectron. Med.* **8** 10
[57] Li H-C, Luo K-X, Wang J-S and Wang Q-X 2020 Extrapyramidal side effect of donepezil hydrochloride in an elderly patient a case report *Medicine* **99** e19443
[58] Zhao M, He X, Bi X Y, Yu X J, Gil Wier W and Zang W J 2013 Vagal stimulation triggers peripheral vascular protection through the cholinergic anti-inflammatory pathway in a rat model of myocardial ischemia/reperfusion *Basic Res. Cardiol.* **108** 345
[59] Xue R-Q, Sun L, Yu X-J, Li D-L and Zang W-J 2017 Vagal nerve stimulation improves mitochondrial dynamics via an M3 receptor/CaMKKβ/AMPK pathway in isoproterenol-induced myocardial ischaemia *J. Cell Mol. Med.* **21** 58–71
[60] Timolati F, Ott D, Pentassuglia L, Giraud M-N, Perriard J-C, Suter T M and Zuppinger C 2006 Neuregulin-1 beta attenuates doxorubicin-induced alterations of excitation–contraction coupling and reduces oxidative stress in adult rat cardiomyocytes *J. Mol. Cell Cardiol.* **41** 845–54
[61] Seddon M, Shah A M and Casadei B 2007 Cardiomyocytes as effectors of nitric oxide signalling *Cardiovasc. Res.* **75** 315–26
[62] Martin S R, Emanuel K, Sears C E, Zhang Y-H and Casadei B 2006 Are myocardial eNOS and nNOS involved in the β-adrenergic and muscarinic regulation of inotropy? A systematic investigation *Cardiovasc. Res.* **70** 97–106
[63] Zhou Y, Varadharaj S, Zhao X, Parinandi N, Flavahan N A and Zweier J L 2005 Acetylcholine causes endothelium-dependent contraction of mouse arteries *Am. J. Physiol. Heart Circ. Physiol.* **289** H1027–H32
[64] Boycott H E, Nguyen M-N, Vrellaku B, Gehmlich K and Robinson P 2020 Nitric oxide and mechano-electrical transduction in cardiomyocytes *Front. Physiol.* **11** 606740
[65] Kalivendi S V, Kotamraju S, Zhao H, Joseph J and Kalyanaraman B 2001 Doxorubicin-induced apoptosis is associated with increased transcription of endothelial nitric-oxide synthase effect of antiapoptotic antioxidants and calcium *J. Biol. Chem.* **276** 47266–76
[66] Kuwabara M, Kakinuma Y, Ando M, Katare R G, Yamasaki F, Doi Y and Sato T 2006 Nitric oxide stimulates vascular endothelial growth factor production in cardiomyocytes involved in angiogenesis *J. Physiol. Sci.* **56** 95–101
[67] Lavin B, Gómez M, Pello O M, Castejon B, Piedras M J, Saura M and Zaragoza C 2014 Nitric oxide prevents aortic neointimal hyperplasia by controlling macrophage polarization *Arterioscler. Thromb. Vasc. Biol.* **34** 1739–46
[68] Sun X, Song Y, Xie Y, Han J, Chen F, Sun Y, Sui B and Jiang D 2021 Shenlijia attenuates doxorubicin-induced chronic heart failure by inhibiting cardiac fibrosis *Evid Based Complement Alternat. Med.* **2021** 1–13
[69] Sun X, Chen G, Xie Y, Jiang D, Han J, Chen F and Song Y 2020 Qiliqiangxin improves cardiac function and attenuates cardiac remodelling in doxorubicin-induced heart failure rats *Pharm. Biol.* **58** 417–26
[70] Thatcher S, Yiannikouris F, Gupte M and Cassis L 2009 The adipose renin–angiotensin system role in cardiovascular disease *Mol. Cell. Endocrinol.* **302** 111–7
[71] Wang X, Meng X, Meng L, Guo Y, Li Y, Yang C, Pei Z, Li J and Wang F 2022 Joint efficacy of the three biomarkers SNCA, GYPB and HBG1 for atrial fibrillation and stroke Analysis via the support vector machine neural network *J. Cell Mol. Med.* **26** 2010–22
[72] El-Naggar A E, El-Gowilly S M and Sharabi F M 2018 Possible ameliorative effect of ivabradine on the autonomic and left ventricular dysfunction induced by doxorubicin in male rats *J. Cardiovasc. Pharmacol.* **72** 22–31
[73] Wang Y-X and Korth M 1995 Effects of doxorubicin on excitation-contraction coupling in guinea pig ventricular myocardium *Circ. Res.* **76** 645–53
[74] Zhao C Y, Greenstein J L and Winslow R L 2016 Roles of phosphodiesterases in the regulation of the cardiac cyclic nucleotide cross-talk signaling network *J. Mol. Cell Cardiol.* **91** 215–27
[75] Kim G E and Kass D A 2017 Cardiac phosphodiesterases and their modulation for treating heart disease *Heart Failure* (*Handbook of Experimental Pharmacology* vol 243) (Springer) pp 249–69
[76] Zhang J, Simpson P C and Jensen B C 2021 Cardiac α1A-adrenergic receptors emerging protective roles in cardiovascular diseases *Am. J. Physiol. Heart Circ. Physiol.* **320** H725–H33
[77] Mohl M C *et al* 2011 Regulation of murine cardiac contractility by activation of α1A-adrenergic receptor-operated Ca2+ entry *Cardiovasc. Res.* **91** 310–9
[78] Sato M *et al* 2018 α1A-Adrenoceptors activate mTOR signalling and glucose uptake in cardiomyocytes *Biochem. Pharmacol.* **148** 27–40
[79] Kolter M, Ott M, Hauer C, Reimold I and Fricker G 2015 Nanotoxicity of poly(n-butylcyano-acrylate) nanoparticles at the blood–brain barrier, in human whole blood and *in vivo J. Control. Release* **197** 165–79
[80] Kumar S, Marfatia R, Tannenbaum S, Yang C and Avelar E 2012 Doxorubicin-induced cardiomyopathy 17 years after chemotherapy *Texas Heart Inst. J.* **39** 424–7